Article

Quasi-Stationary Strength of ECAP-Processed Cu-Zr at 0.5 T_m

Wolfgang Blum [1,*], Jiří Dvořák [2], Petr Král [2], Philip Eisenlohr [3] and Vaclav Sklenička [2]

[1] Department of Materials Science, Institute I, University of Erlangen-Nuremberg, Martensstr. 5, D-91058 Erlangen, Germany
[2] Institute of Physics of Materials, Czech Academy of Sciences, Žižkova 22, CZ-616 62 Brno, Czech Republic; dvorak@ipm.cz (J.D.); pkral@ipm.cz (P.K.); sklen@ipm.cz (V.S.)
[3] Chemical Engineering and Materials Science, Michigan State University, East Lansing, MI 48824, USA; eisenlohr@egr.msu.edu
* Correspondence: wolfgang.blum@fau.de

Abstract: The influence of the grain structure on the tensile deformation strength is studied for precipitation-strengthened Cu-0.2%Zr at 673 K. Subgrains and grains are formed by equal channel angular pressing (ECAP) and annealing. The fraction of high-angle boundaries increases with prestrain. Subgrains and grains coarsen during deformation. This leads to softening in the quasi-stationary state. The initial quasi-stationary state of severely predeformed, ultrafine-grained material exhibits relatively high rate-sensitivity at relatively high stresses. This is interpreted as a result of the stress dependences of the quasi-stationary subgrain size and the volume fraction of subgrain-free grains.

Keywords: Cu-Zr; ECAP; deformation; quasi-stationary; subgrains; grains; coarsening

1. Introduction

Deformation of single crystals and large-grained polycrystals leads to generation of dislocations and subgrains with low-angle boundaries (LABs). Dynamic recovery counteracts the defect generation. The state at which the rate $\dot{\rho}^+$ of increase of density ρ of free dislocations approximately equals the rate $\dot{\rho}^-$ of ρ-decrease,

$$\dot{\rho}^+ \approx \dot{\rho}^-, \tag{1}$$

is usually called steady state, stationary state or saturation stage (of flow stress) in the literature. We prefer the term quasi-stationary (qs) state [1], because slow changes of microstructure parameters (boundaries [2,3], particles, ...) lead to a drift of the quasi-equilibrium of the qs state that in turn causes slow changes of the qs deformation strength. By definition, there is a spectrum of qs states, depending on the microstructural parameters other than ρ. The qs states are important as upper limits of deformation strength at given structure of grains and particles.

The present work deals with the strength of a Cu-Zr alloy that is stabilized by particles and processed by equal channel angular pressing (ECAP). It is well known that ECAP processing leads into a qs state with refined grains and saturated hardness (compare [4–7]). This holds also for Cu-Zr [8–10]. When the ECAP-processed material is subjected to creep at elevated temperature of 673 K, new qs states are developed. The creep ductility is significantly enhanced compared to the coarse-grained (cg) alloy while the creep rate remains fairly low and has relatively low stress sensitivity. In the following section, we treat the evolution of deformation strength and microstructure of ECAP-processed Cu-Zr at 673 K in detail on updated data basis with the goal to better understand how grain refinement influences the qs deformation strength. We discuss the proposition that the qs strength of ultrafine-grained (ufg)

Cu-Zr significantly depends on the stress-dependent qs fraction of subgrain-free grains. There are indications that the variation of this fraction with stress may explain the relatively low stress sensitivity (high rate sensitivity) of the qs strength of grain-refined ufg Cu-Zr.

2. Experimental Details

Processing, microstructure, and creep testing have been described before [10]. The starting material was (cg) Cu-0.2 mass%Zr. Its material parameters are approximated by those of pure Cu provided in the data compilation of Frost and Ashby [11]: Burgers vector $b = 2.56 \times 10^{-10}$ m, elastic shear modulus $G = 3.58 \times 10^4$ MPa, melting point $T_m = 1356$ K. The cg material was homogenized for 24 h at 1073 K and hot rolled. Billets of this material were solution treated at 1233 K for 1 h to give an initial grain size of 3.5×10^{-4} m. The billets were predeformed by p passes of equal channel angular pressing (ECAP, Figure 1) at room temperature on route B_C to refine the grains. The predeformed material is called pCu-Zr. Due to particle hardening the grain size of the material is stable against static annealing at temperatures exceeding the test temperature 673 K [12]. The thermal treatment consisted of storage of the predeformed material at room temperature for up to several years followed by heating to and holding at T for a few hours before deformation.

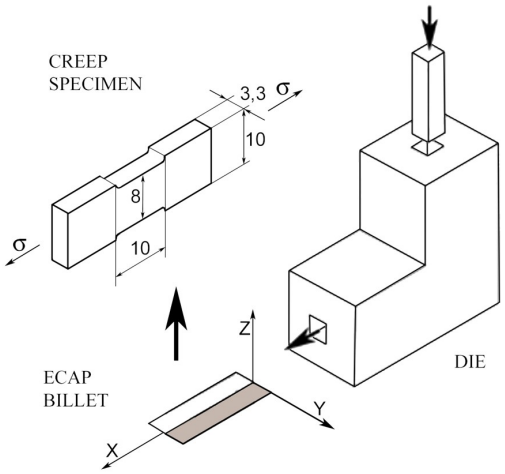

Figure 1. From ECAP billet to tensile creep specimen (numbers: lengths/mm).

Flat tensile creep specimens with gauge length l_0 and cross section S_0 were prepared as illustrated in Figure 1. Deformation in creep mode occurred in tension at temperature $T = 673\,\mathrm{K} = 0.5\,T_m$ upon applying a load F, corresponding to an engineering stress $\sigma_{eng} = F/S_0$. The change Δl of the length was measured using LVDTs (from Hottinger Baldwin Messtechnik GmbH, Darmstadt, Germany) attached to the tensile rods near the specimen. The "true" strain ϵ results as $\ln((l_0 + \Delta l)/l_0)$ (Elastic contribution to Δl are neglected here because it is relatively small and nearly constant at constant F so that the elastic contribution $\dot{\epsilon}_{el}$ to the measured rate $\dot{\epsilon}$ is generally negligible). Due to volume constancy and under uniform deformation of the gauge length $l = l_0 + \Delta l$, the cross section S varies as $S = S_0\, l_0/l = S_0 \exp(-\epsilon)$ and the "true" stress σ, given by F/S, increases with strain as

$$\sigma = \sigma_{eng} \exp(\epsilon). \tag{2}$$

Observations of the grain structure were made by electron microscopy. Orientation maps derived from electron backscatter diffraction (EBSD, device from Oxford Instruments, High Wycombe, United Kingdom) were used to determine the grain size d as mean value of the spacings d_i, $i = 1, 2, 3, \ldots$, of HABs between crystallites with misorientations $\geq 15°$ determined along test lines. Transmission electron microscopy (TEM) images (microscope from JEOL Ltd., Tokyo, Japan) were

used to analogously determine the subgrain size w as mean value of the spacings w_i of boundaries of any kind.

3. Results

3.1. Influence of Predeformation

With increasing predeformation p the deformation strength of pCu-Zr saturates, because the areal fraction f_{HAB} of high-angle boundaries (HABs) increases up to a saturation level [9] where a qs state is established due to dynamic equilibrium of storage and dynamic recovery of dislocations. This statement is consistent with the observation that the Vickers hardness saturates with increasing predeformation p at $HV \approx 180$ [9]; using the formula $\sigma/\mathrm{MPa} \approx 3\,HV$, this corresponds to a saturation flow stress of 540 MPa in ECAP. An increase of f_{HAB} enhances storage as well as recovery of dislocations because HABs are stronger dislocation obstacles and better dislocation sinks than LABs. The net effect on deformation strength depends on whether storage or recovery are the dominant factors (compare, e.g., [13]).

Figure 2 shows exemplary curves of the evolution of deformation resistance with strain at constant engineering stress $\sigma_{\mathrm{eng}} = 150\,\mathrm{MPa}$ for different amounts p of ECAP predeformation. Deformation starts with application of the load F, and continues in creep mode when the creep stress σ_{eng} has been reached. The starting phase of the tests is connected with work hardening as is visible from the sharp decrease of strain rate $\dot{\epsilon}$ with ϵ. After strains of 0.02 to 0.05 the rate $\dot{\epsilon}$ increases. A trivial reason for $\dot{\epsilon}$-increase lies in the increase of σ with ϵ (Equation (2)) causing the creep rate to increase in the qs state as $\dot{\epsilon} \propto \sigma^{n_{\mathrm{qs}}}$ where n_{qs} is the qs value of the stress exponent. The dotted line in Figure 2 shows that for severely predeformed Cu-Zr with $p \geq 8$ practically all of the $\dot{\epsilon}$-increase can be attributed to the increase of σ when $n_{\mathrm{qs}} = 6$ (as reported before [9]). This means that at $\sigma_{\mathrm{eng}} = 150\,\mathrm{MPa}$

- the specimens of 8/12Cu-Zr begin to deform in their qs state right from low strains in the order of 0.02, and
- changes of boundary and particle structures are negligible.

At about half the fracture strain the $\dot{\epsilon}$-increase accelerates. This indicates formation of local stress concentrations by external and internal necking during the fracture process.

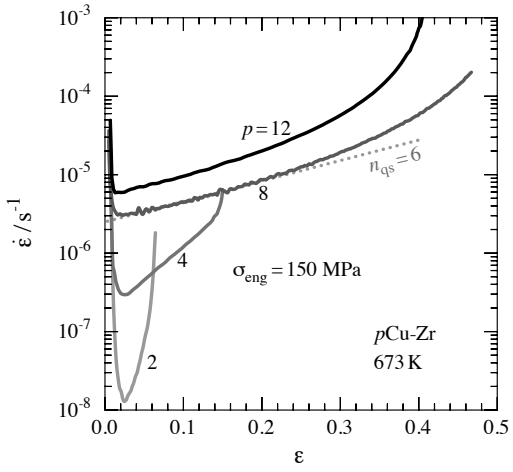

Figure 2. $\dot{\epsilon}$ versus ϵ for pCu-Zr at 673 K, $\sigma_0 = 150\,\mathrm{MPa}$ in tension at constant load; dotted line: increase of $\dot{\epsilon}$ expected from increase of σ for $n_{\mathrm{qs}} = 6$.

The less strongly predeformed specimens 4Cu-Zr and 2Cu-Zr exhibit a distinctly steeper increase of $\dot{\epsilon}$ with ϵ. To find the reason for that, it is useful to display the creep process in the qs region near the minimal creep rate, i.e., the creep between the work hardening period and the fracture period, in the

$\log \dot{\epsilon} - \log \sigma$-field (Figure 3). According to Equation (2), $\log \sigma$ increases linearly with ϵ. The scale-bars in Figure 3 show the extension of a strain interval $\Delta\epsilon$ of 0.5. Figure 3e confirms that most of the curves for 8Cu-Zr have slopes near $n_{qs} = 6$ in the qs range above 150 MPa and follow a common trend given by the dashed black line. For 12Cu-Zr this behavior is even more perfectly pronounced, indicating better homogeneity of the initial microstructure.

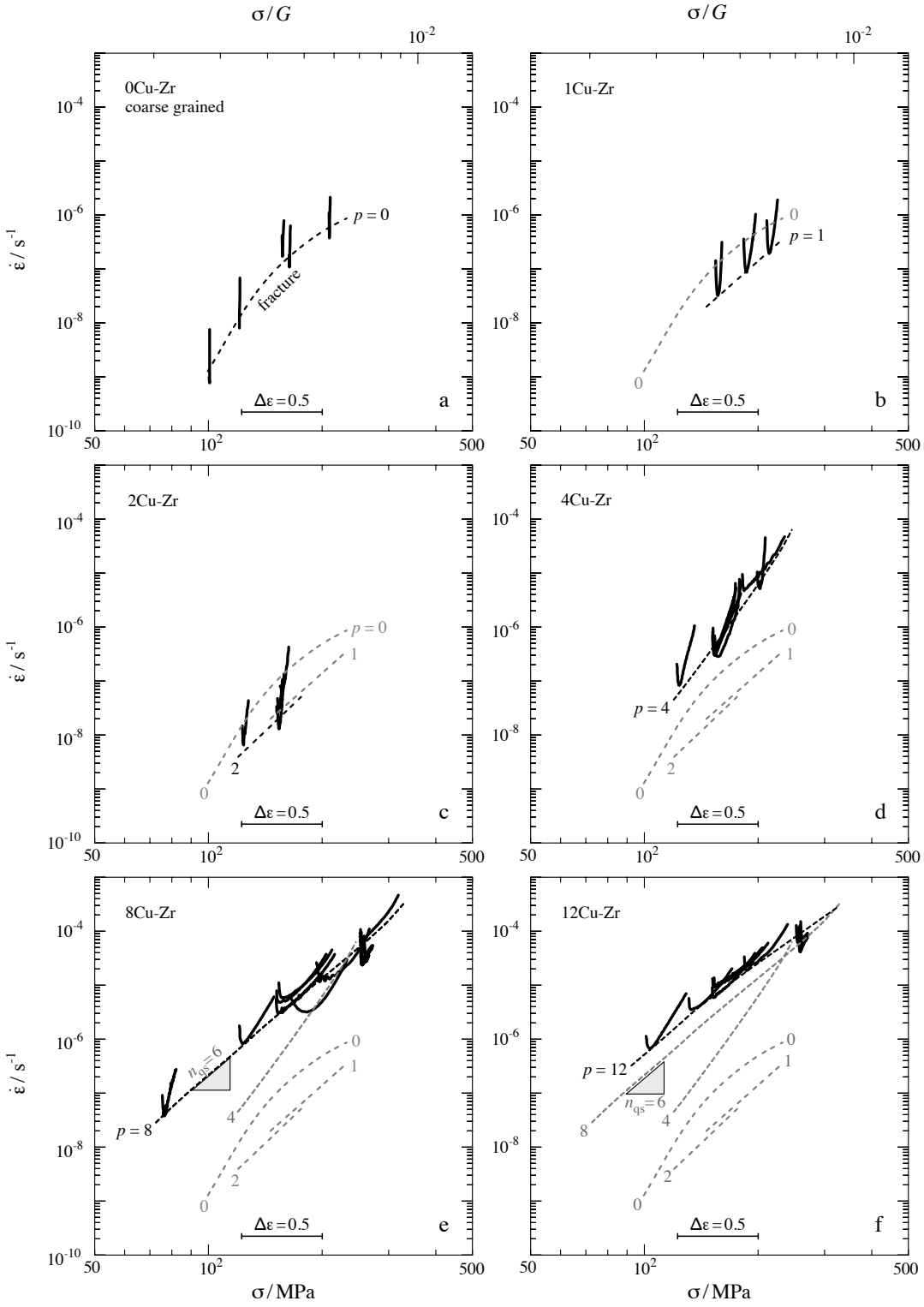

Figure 3. $\dot{\epsilon}$ versus σ for pCu-Zr at 673 K in tension at constant load.

For lower stresses $\sigma < 150$ MPa and for pCu-Zr with $p \leq 4$ the slopes in Figure 3 are distinctly higher and different curves do not merge. One reason is tensile fracture. Figure 3a shows that fracture occurs in cg Cu-Zr (i.e., pCu-Zr with $p = 0$), before a qs region has been developed. This means that the qs deformation strength cannot be measured in tension. Thus, the experimental values of the minimal creep rate are determined by fracture, and therefore constitute only upper bounds of the qs deformation strength. The same holds for predeformed pCu-Zr with $p = 1$ to 4. (To determine the qs deformation strength, compression tests would be required in these cases in order to delay or suppress fracture). For ufg 8/12Cu-Zr the strains are too large to explain the non-merging of the curves at low σ by fracture processes. Therefore this effect must be due to softening during creep. In Section 3.3 we provide an explanation of the softening in terms of dynamic coarsening of the microstructure.

In summary, one sees from Figure 3 that the qs deformation strength of Cu-Zr decreases at the test temperature 0.5 T_m when the material is severely predeformed, the grains are refined, and the areal fraction f_{HAB} of boundaries with high-angle character increases during creep.

3.2. Microstructure of 8Cu-Zr

3.2.1. Before Creep

Heating to and holding at test temperature before creep took a few hours. Figures 4 and 5a illustrate the microstructure of 8Cu-Zr after annealing for a few hours at the test temperature. So these microstructures are representative for the microstructure at start of creep. From a micrograph, such as Figure 4, the initial grain size d_0 of 8Cu-Zr was determined as 4.7×10^{-7} m. From the 8Cu-Zr sample of Figure 5a the initial subgrain size w_0 was determined as 1.5×10^{-7} m. Noting that these are local values that may vary from place to place and from specimen to specimen, the agreement with previously published data [10] and with data from the literature for severely predeformed ufg Cu-Zr [12,14,15] data is considered to be satisfactory. From the empirical formula

$$w_{qs}^{cg} \approx 14\, b\, G/\sigma \tag{3}$$

for cg Cu [16] and the estimate 540 MPa for the saturation strength in ECAP given above one gets a qs subgrain size of 2.4×10^{-7} m. In view of the uncertainty of the empirical factor 14 entering Equation (3), the agreement with the measured w_0 is considered satisfactory, too. This means that w_0 may be interpreted as the qs value of the subgrain size in ufg 8Cu-Zr before creep, that is only marginally influenced by the heating to test temperature.

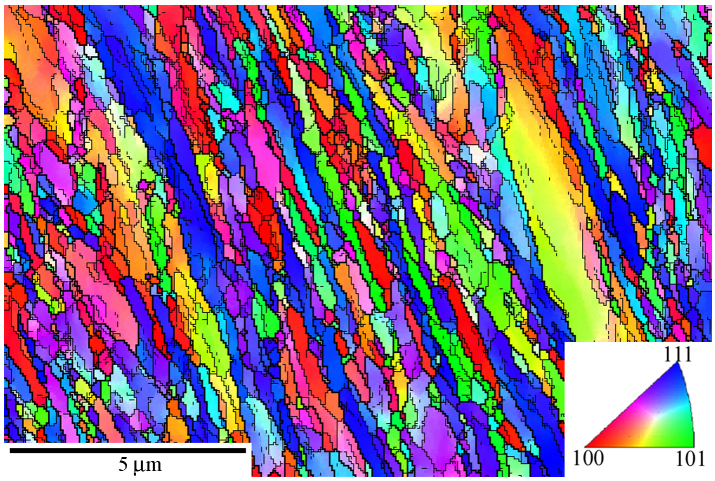

Figure 4. Grain structure map of 8Cu-Zr after 10 h of annealing at 673 K; thin and thick lines: traces of boundaries with misorientation $<$ and $>$ 15°, respectively. Insert: color code for crystallographic grain normals in standard triangle.

Preprints (www.preprints.org) | NOT PEER-REVIEWED | Posted: 6 September 2019 doi:10.20944/preprints201909.0073.v1

Peer-reviewed version available at Metals 2019, 9; doi:10.3390/met9111149

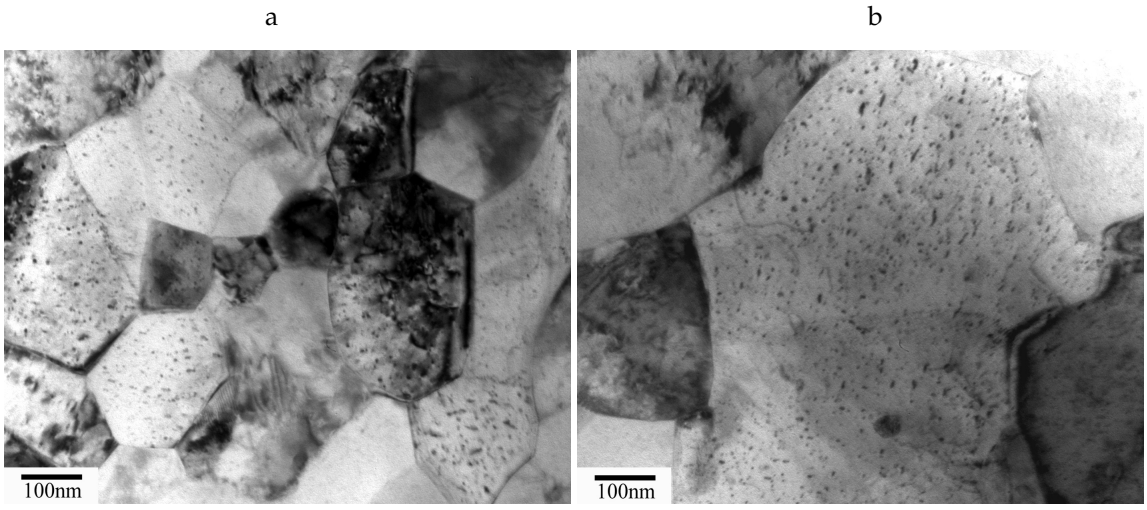

Figure 5. TEM of subgrains and Cu_5Zr-precipitates in 8Cu-Zr after (**a**) annealing for 8 h at 673 K, (**b**) creep at 673 K, $\sigma_{eng} = 150$ MPa to a fracture strain of ≈0.5 (compare curve for $p = 8$ in Figure 2).

The Zr containing particles are essential in restricting grain coarsening [10,12,14]. They are present in homogeneous distribution after SPD ([14] and Figure 5). Figure 6 shows electron diffraction patterns of (a) the Cu matrix with particles and (b) a large particle of composition Cu_5Zr. A rough estimate based on Equations (7)–(13) in [17] (using a mean particle radius of 4 nm, number of particles per area of TEM foil equal to 10, typical foil thickness of 200 nm) yields an Orowan stress for particle hardening of about 150 MPa at room temperature. However, at the test temperature the tiny particles are easily overcome by local and general climb of dislocations so that the particle hardening term is greatly reduced [17]. In the following, we neglect the direct influence of particles on the stress sensitivity of the deformation strength.

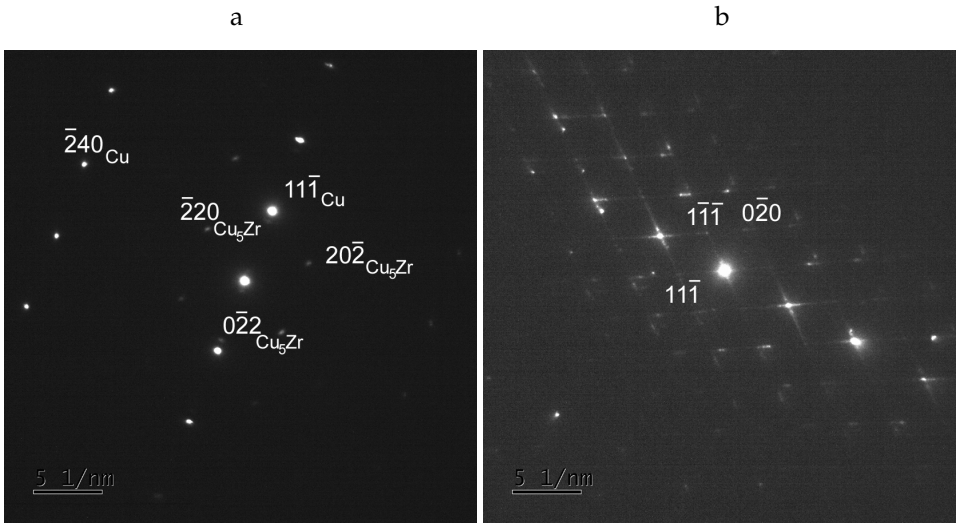

Figure 6. Diffraction patterns of (**a**) Cu matrix (strong reflections) with Cu_5Zr particles (weak reflections) and (**b**) a large Cu_5Zr particle.

The spacing plot of Figure 7 shows w_0 and d_0 together with the qs spacings $\approx bG/\sigma$ of dislocations and w_{qs}^{cg} of boundaries in cg Cu. We assume that the qs spacings for cg Cu are valid also for Cu-Zr. It is interesting to note that at low stresses the (dotted) qs dislocation spacing would be similar to the initial boundary spacing w_0, meaning that the subgrains will tend to be virtually dislocation-free in the beginning of creep. This will increase the mobility of boundaries. As w_0 is smaller than $w_{qs}^{cg}(\sigma)$ in the whole stress interval of creep (Figure 7), the subgrains will tend to coarsen with strain toward the quasi-stationary value w_{qs}^{cg} as long as the grains provide enough space, i.e., as long as w is smaller than

d. The grey area marks the range of possible subgrain coarsening under the simplifying assumptions that all grains are equiaxed and keep the same size $d = d_0$ throughout deformation. The solid black line marks the qs boundary spacing in ufg 8Cu-Zr under these conditions. If this line were exactly valid, all grains would become subgrain-free during deformation for stresses < 270 MPa. However, that is unrealistic because of (i) the wide distribution of HAB spacings (Figure 9) and (ii) dynamic grain growth (see below).

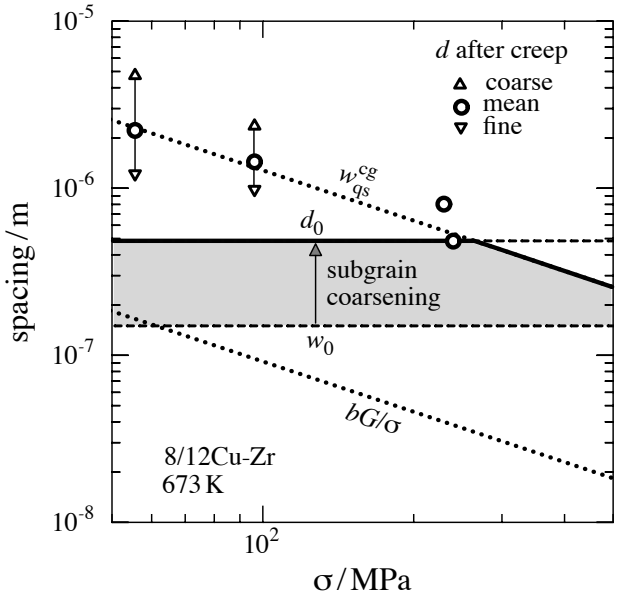

Figure 7. Initial spacings w_0 (all boundaries) and d_0 (HABs only) in pCu-Zr with $p \geq 8$ in comparison to the qs spacings w_{qs}^{cg} of subgrains (Equation (3)) and $\approx b\,G/\sigma$ of free dislocations expected in coarse-grained Cu-base material; circles: HAB-spacings after deformation, triangles: HAB-spacings in regions with relatively fine and coarse grains, respectively; grey area: range of subgrain coarsening for $d = d_0$.

3.2.2. After Creep

Figure 8 shows grain structures after creep at low σ. There is a mixture of large and fine grain sections. The largest ones are much coarser than in the initial state (Figures 4 and 7). Coarsening is also seen from the TEM micrograph of Figure 5b after fracture at σ_{eng}=150 MPa in comparison to Figure 5a taken before creep. However, this is probably mainly due to subgrains growing from w_0 (Figure 5a) in the attempt to attain the qs spacing w_{qs}^{cg}. Figure 9 shows the distributions of individual HAB-spacings determined from Figures 4 and 8. We will use them as rough experimental input to the model presented in Section 4.

Comparison of Figure 5a,b shows no indications for significant coarsening of particles during creep. So we assume that the stabilization of the grain structure by particles will essentially persist in creep.

Preprints (www.preprints.org) | NOT PEER-REVIEWED | Posted: 6 September 2019 doi:10.20944/preprints201909.0073.v1

Peer-reviewed version available at Metals 2019, 9; doi:10.3390/met9111149

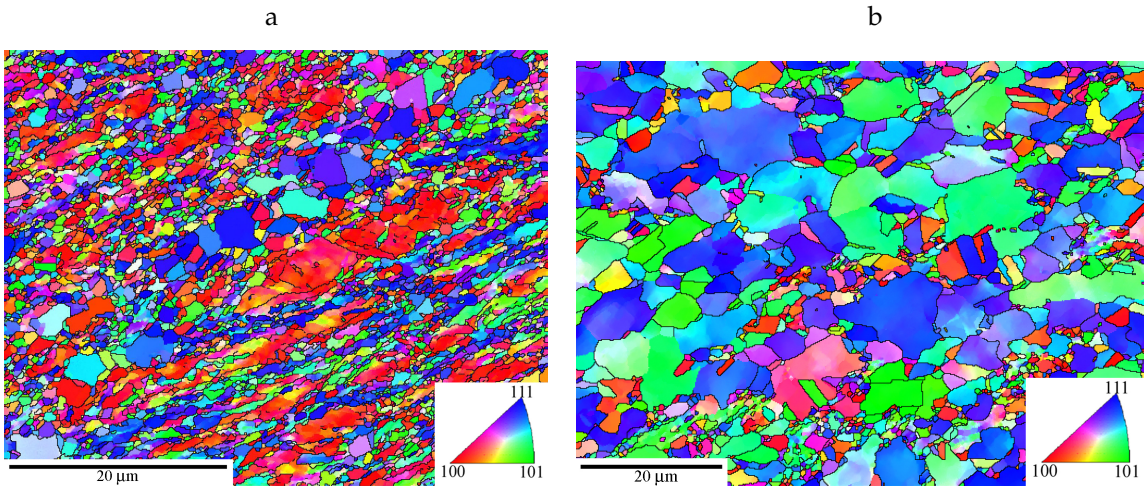

Figure 8. Coarsened grains after slow creep at σ_{eng} = (**a**) 75 MPa and (**b**) 50 MPa (grey triangles in Figure 7); slight color variations in some coarsened grains indicate subgrain formation during creep; insert: color code for crystallographic grain normals in standard triangle.

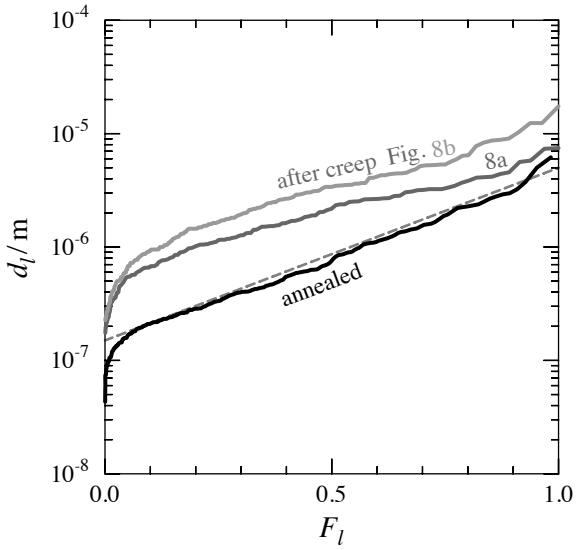

Figure 9. Individual HAB-spacings d_l ($l = 1, 2, \ldots$) versus cumulative spacing fraction F_l evaluated for 8Cu-Zr in annealed state from Figure 4 and after slow creep from Figure 8a,b. Grey dashed line: linear approximation for annealed state.

3.3. Strength Evolution of 8/12Cu-Zr with Strain

Figure 10 displays the $\dot{\epsilon}$-evolution of ufg 8Cu-Zr from the overview of Figure 3e in greater detail as function of strain ϵ. For comparison, the grey dotted lines show the increase of $\dot{\epsilon}$ with ϵ expected for qs deformation with $n_{qs} \approx 6$ at constant σ_{eng}. The scatter in the series of tests at $\sigma_{eng} = 250$ MPa indicates that the thermomechanical pretreatment was not perfect and led to some variations of microstructures and strengths. The intermediate σ_{eng}-increase to 83 MPa in the test starting at 75 MPa causes a jump in the qs level of $\dot{\epsilon}$ at $\epsilon \approx 0.15$ (see black squares) which corresponds to $n_{qs} = 5.3$. This is in reasonable agreement with $n_{qs} \approx 6$. At high (true) stresses $\sigma > 270$ MPa and strain rates $> 10^{-4}\,s^{-1}$ the exponent n_{qs} appears to gradually increase with σ beyond 6. This is seen from the test of Figure 11 with a series of load reductions compensating the increase of σ with ϵ (Equation (2)). When the abscissa ϵ in Figure 11a is exchanged for σ in Figure 11b, all the branches with $\sigma_{eng} < 250$ MPa shift to the left and superimpose. A common $\dot{\epsilon}$–ϵ line describes both the superimposed curves and their (dashed) connection to the final branch with $\sigma_{eng} = 250$ MPa. The slope of the dashed connection is given by $n_{qs} = 10.4$ at $\sigma > 275$ MPa.

Preprints (www.preprints.org) | NOT PEER-REVIEWED | Posted: 6 September 2019 doi:10.20944/preprints201909.0073.v1

Peer-reviewed version available at Metals 2019, 9; doi:10.3390/met9111149

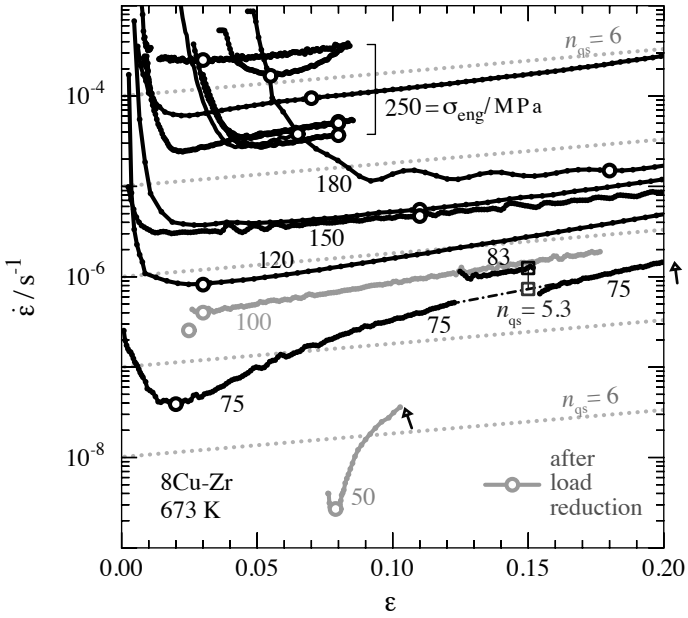

Figure 10. $\dot{\epsilon}$ of 8Cu-Zr as function of ϵ at constant σ_{eng}; black circles: identified qs rates; grey: after σ_{eng}-reduction of from 250 MPa; see Figure 8 for microstructure at black arrows.

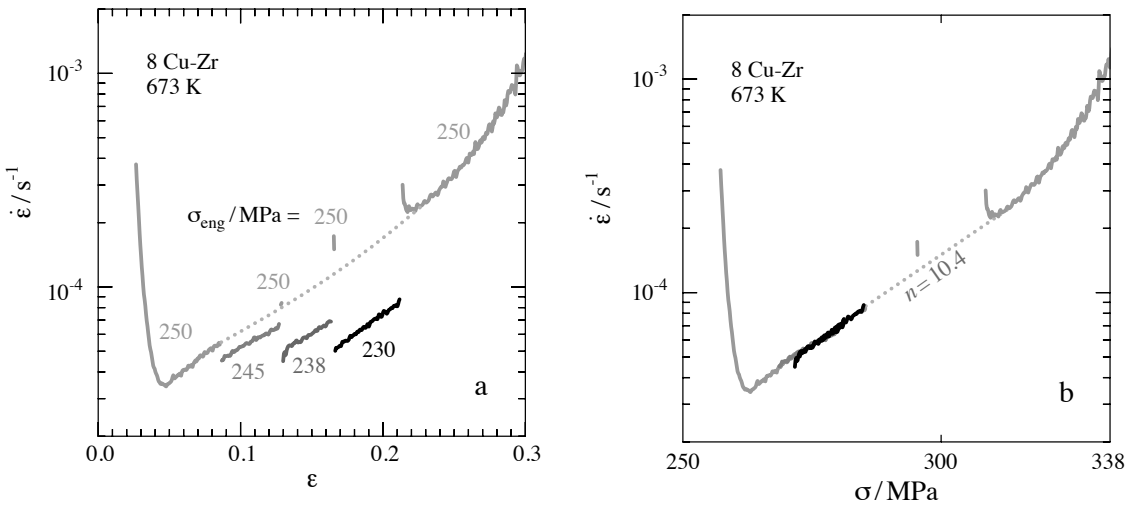

Figure 11. $\dot{\epsilon}$-evolution of 8Cu-Zr as function of (**a**) ϵ, (**b**) $\sigma = \sigma_{eng}\ \exp(\epsilon)$ in test with σ_{eng}-reductions of increasing magnitude to keep $\sigma = \sigma_{eng}\ \exp(\epsilon)$ about constant.

At low σ<150 MPa the qs strength evolution can no longer be explained only in terms of the slow increase of σ at constant σ_{eng} and fracture (see Figures 3 and 10. Therefore changes in the subgrain/grain structures must be invoked. This corresponds to the observed dynamic coarsening of subgrains and grains (Figure 7, Sections 3.2.1 and 3.2.2).

3.4. Quasi-Stationary Strength of 8/12Cu-Zr

The circles in Figure 10 indicate the quasi-stationary strengths of ufg Cu-Zr at the grain/phase structure present at the beginning of creep. Their choice results from a compromise of

- providing enough strain to fill the material with a qs dislocation structure (spacing of free dislocations and subgrain size) while
- avoiding grain coarsening at large strains.

Taking into account that subgrain growth by migration of LABs is a relatively fast process needing strains in the order of 0.05 to 0.1 and that only limited subgrain growth is possible before all LABs were absorbed at the HABs of mean spacing d_0 (Figure 7), we expect that at the rather low strains of the qs states marked by circles in Figure 10 only marginal grain coarsening will have happened and that sufficiently small grains will have become subgrain-free by subgrain coarsening, except perhaps at the lowest stresses. Figure 12a shows the circles from Figure 10 as function of stress σ for ufg 8Cu-Zr. Within scatter, the qs strengths confirm the power law with a stress exponent $n_{qs} = 6$, already mentioned in Section 3.1, for the stress range 70 MPa $< \sigma <$ 260 MPa. The square symbols from the load change test demonstrate the moderate softening effect resulting from dynamic (sub)grain coarsening mentioned before (Figure 7). An analogous procedure as for 8Cu-Zr leads to Figure 12b for ufg 12Cu-Zr. There is no significant difference between 8Cu-Zr and 12Cu-Zr except lesser scatter for 12Cu-Zr at (true) stresses near 270 MPa (corresponding to $\sigma_{eng} = 250$ MPa), probably due to better homogeneity of the grain structure of 12Cu-Zr.

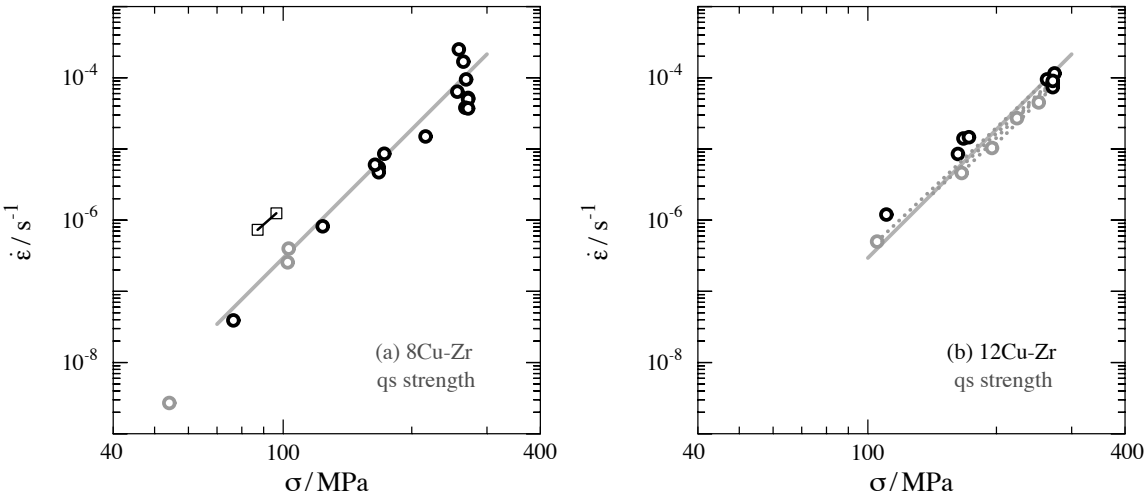

Figure 12. Quasi-stationary strengths of (**a**) 8Cu-Zr (symbols from Figure 7) and (**b**) 12Cu-Zr; grey dotted lines connect data from the same test.

4. Discussion

The primary transients in ufg materials are usually small because the high density of HABs limits the free path of dislocations effectively and leads to high rates of dislocation generation. They are roughly estimated [18] as $d\rho^+/d\epsilon = 2M/(b\Lambda)$ with $\Lambda \approx d_0 \approx 5 \times 10^{-7}$ m and Taylor factor $M = 3$ for polycrystals. Without concurrent dynamic recovery it needs a strain interval $\Delta\epsilon^+ \approx M^{-1}\,(b/d)\,(\sigma/G)^2\,\Delta\rho^+$ to generate the full qs dislocation density $\rho_{qs} \approx b^{-2}\,(\sigma/G)^2$ in grains of size $d = d_0$. This means that at a stress of 150 MPa a plastic strain of $\Delta\epsilon^+ = 0.011$ is sufficient to generate the full qs dislocation density. This value is consistent with the primary transients extending over strain intervals > 0.01 in creep at $\sigma_{eng} = 150$ MPa (Figure 10) and confirms that a qs state in the sense of Equation (1) is reached shortly after the $\dot{\epsilon}$-minimum.

The aim of the present work is to learn more about the influence of the grain structure on the qs strength. As shown above, the high value of f_{HAB} has a softening effect (Section 3.1) and

Preprints (www.preprints.org) | NOT PEER-REVIEWED | Posted: 6 September 2019 doi:10.20944/preprints201909.0073.v1

Peer-reviewed version available at Metals 2019, 9; doi:10.3390/met9111149

leads to a relatively high rate sensitivity (equivalent to low stress sensitivity n_{qs}) of the qs strength (Section 3.4). The qs stress exponent $n_{qs} \approx 6$ and a high activation energy remind one of the power laws of steady state creep that are explained by specific mechanisms of qs creep, characterized by a certain stress exponent n_{qs} and rate sensitivity $1/n_{qs}$ (see, e.g., [19–21]). For example, mechanisms 1 and 2 in Figure 13a might represent climb-controlled steady state creep and superplastic deformation, respectively. Following this approach, the power law range in Figure 12 would correspond to some mechanism 2.

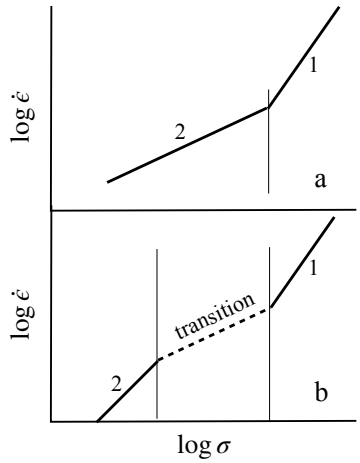

Figure 13. Mechanisms 1 and 2 of qs deformation with (**a**) abrupt, (**b**) smooth transition.

However, there is an alternative possibility [22]. The investigated region with relatively high rate sensitivity may represent a smooth *transition* between a mechanism 1 dominating at high σ and a mechanism 2 dominating at low σ (Figure 13b). A transition region must be expected from the fact that the spacings of HABs have a wide distribution due to coexistence of small and large grains. According to the microstructural data of Figure 7, mechanism 1 would represent qs deformation with subgrain-bearing grains, while mechanism 2 would represent qs deformation with subgrain-free grains (This makes a qualitative difference to Ghosh and Raj [23] who studied the influence of a distribution of grain sizes in relation to the transition between superplastic and normal behavior, but assumed that both mechanisms of deformation are concurrently active in each grain). In the (dashed) transition region both types of grains would be present. In qualitative form this possibility has already been applied to microcrystalline Cu at 0.35 T_m [24]. A semi-quantitative model was provided in [25] and applied to microcrystalline Cu at 0.42 T_m [26]. To apply this model to the present case we need the qs strengths of grains with and without subgrains and the distribution of grain volumes $i = 1, 2, \ldots$ with spacings d_i between the HABs for ufg Cu-Zr at 0.50 T_m. This warrants assumptions based on educated guesses. Following [25,26] we make these choices:

- The cumulative volume fraction F_d with HAB-spacings $\leq d$ is described by the thin straight line in Figure 9 (grey, dashed).
- The qs strength of *subgrain-free* grains is quantified by the relation

$$\dot{\epsilon} \propto d^4 \sigma^8 \tag{4}$$

  from [27]; the f-factors were set to 0.19 (f-factors $= 1$ apply in the limiting case where all dislocations are lying at HABs, all are in dipolar configuration ready for recovery, and have unrelaxed stress fields; as this is unrealistic, f-values distinctly less than 1 are sensible). This choice yields the two dashed grey lines in Figure 14a for the present F_d and the limiting assumptions of equal stress (iso-stress) or equal strain rate (iso-rate) in all grains.
- The qs strength of crystal volumes *with* subgrains of size $w_{qs}^{cg}(\sigma)$ is estimated by the power law $\dot{\epsilon} \propto \sigma^{15}$ (dotted line in Figure 14a). The exponent 15 is motivated by the increase of n_{qs} with

stress for $\sigma > 270$ MPa (Figure 12). The position of the line is supported by the result for 2Cu-Zr in Figure 2: The grain size in 2Cu-Zr is so large that all grains contain subgrains; at 150 MPa the upper bound of the initial qs strain rate of 2Cu-Zr is near $10^{-8}\,s^{-1}$ (Figures 2 and 3c); this is consistent with the (grey dotted) estimate for subgrain-containing grains in Figure 14a.

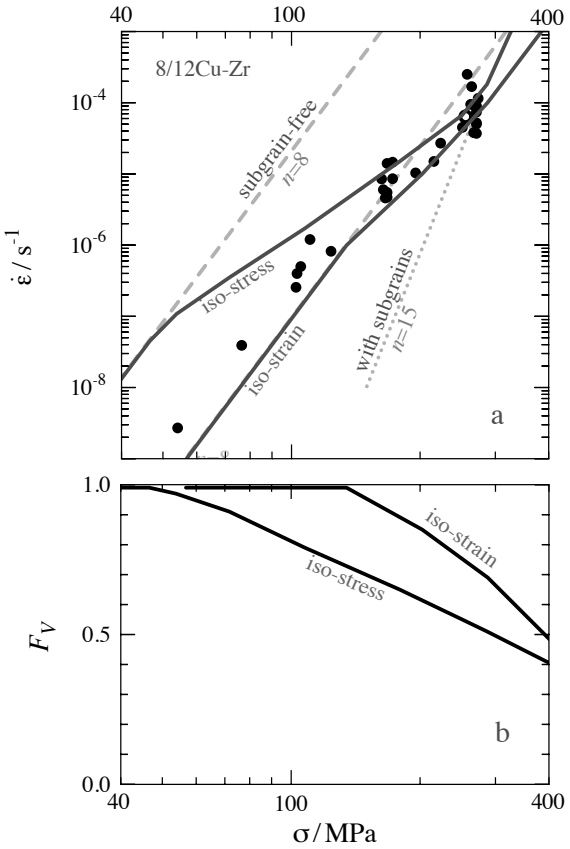

Figure 14. (**a**) Strain rate and (**b**) volume fraction of subgrain-free grains as function of stress σ in qs deformation; filled circles: qs data for 8/12Cu-Zr from Figure 12a,b, solid lines: model.

The solid black lines in Figure 14 show the result of the modeling. The iso-rate assumption enforces a redistribution of stress; σ-concentration to hard grains reduces the stresses in soft grains. This stress shielding hinders deformation of large, soft grains and so raises the flow stress level compared to the iso-stress case. The realistic situation lies between the two limits of iso-stress and iso-rate. Comparison of the model lines with the measured data shows reasonable agreement, in particular with regard to the minimal stress sensitivity n_{qs} (maximal rate sensitivity $1/n_{qs}$) in the transition from subgrain-free to subgrain-containing grains.

We note that the difference between the two model lines is rather small in the transition region and that the choice of the solid grey straight F_d-line in Figure 9 has relatively little influence there. The reason may lie in a compensation effect. On the one hand, subgrain-free grains deform faster at a given stress when their grain size d increases (Equation (4)). On the other hand, the fraction of subgrain-free grains decreases with increasing d as more grains develop subgrains. This means that grain coarsening may not always have the dramatic effect expected from the d^4-term in relation (4). At low σ and $\dot{\varepsilon}$ the situation is unclear because subgrains as well as grains coarsen during creep and the microstructural data are not precise enough for modeling. Therefore, we refrain from a detailed discussion here.

5. Summary

- The quasi-stationary (qs) strength of particle-strengthened ufg Cu-Zr prepared by ECAP and annealing was determined at $0.5\,T_m$ in deformation (creep) at constant load.
- At $\sigma_{eng} = 150\,\text{MPa}$ increase of the fraction f_{HAB} of high-angle boundaries (HABs) leads to softening and ductilization. So HABs have a net softening effect at test conditions.
- The (HAB) grain structure of ufg Cu-Zr is relatively stable at $0.5\,T_m$. At low $\dot{\varepsilon}$ dynamic grain coarsening sets in and leads to softening.
- The initial qs strength of ufg Cu-Zr measured before massive grain coarsening is described by a power law $\dot{\varepsilon} \propto \sigma^n$ with stress exponent $n_{qs} \approx 6$, corresponding to a relatively high rate sensitivity $1/n_{qs} \approx 1/6 = 0.17$, around $\dot{\varepsilon} = 10^{-4}\,\text{s}^{-1}$ and the relatively high stress $\sigma = 170\,\text{MPa} = 4.7 \times 10^{-3}\,G$.
- Analysis of the grain structure indicates that an increasing fraction of small grains becomes subgrain-free in the qs state as the stress decreases.
- The relatively high qs rate sensivity of ufg Cu-Zr is modeled as a result of the variation of the fraction of relatively soft subgrain-free grain volume with stress.

Author Contributions: Conceptualization, W.B. and P.K.; methodology, V.S., J.D., P.K. and P.E.; software, W.B. and P.E.; validation, P.K., J.D.; formal analysis, W.B.; investigation, V.S., J.D., P.K.; resources, J.D.; data curation, J.D., P.K. and W.B.; writing–original draft preparation, W.B.; writing–review and editing, W.B., P.K. and P.E.; visualization, W.B; J.D., P.K., W.B. and P.E.; supervision, W.B. and V.S.

Conflicts of Interest: The authors declare no conflict of interest.

Abbreviations

The following abbreviations are used in this manuscript:

qs	quasi-stationary
ECAP	equal channel angular pressing
ufg	ultrafine-grained
cg	coarse grained
LAB	low-angle boundary
HAB	high-angle boundary
TEM	Transmission electron microscopy

References

1. Blum, W.; Dvořák, J.; Král, P.; Eisenlohr, P.; Sklenička, V. What is stationary deformation of pure Cu? *J. Mater. Sci.* **2014**, *49*, 2987–2997. [CrossRef]
2. Mughrabi, H. Implications of non-negligible microstructural variations during steady state deformation. *Z. Metallkd.* **2005**, *96*, 546–551. [CrossRef]
3. Blum, W.; Eisenlohr, P. Structure evolution and deformation resistance in production and application of nanostructured materials—The concept of steady-state grains. *Mater. Sci. Forum* **2011**, *683*, 163–181. [CrossRef]
4. Valiev, R.Z.; Korznikov, A.V.; Mulyukov, R.R. Structure and properties of ultrafine-grained materials produced by severe plastic deformation. *Mater. Sci. Eng. A* **1993**, *168*, 141–148. [CrossRef]
5. Iwahashi, Y.; Horita, Z.; Nemoto, M.; Langdon, T. The process of grain refinement in equal-channel angular pressing. *Acta Mater.* **1998**, *46*, 3317–3331. [CrossRef]
6. Valiev, R.; Islamgaliev, R.; Alexandrov, I. Bulk nanostructured materials from severe plastic deformation. *Progr. Mater. Sci.* **2000**, *45*, 103–189. [CrossRef]
7. Estrin, Y.; Vinogradov, A. Extreme grain refinement by severe plastic deformation: A wealth of challenging science. *Acta Mater.* **2013**, *61*, 782–817. [CrossRef]
8. Kral, P.; Svoboda, M.; Dvorak, J.; Kvapilova, M.; Sklenicka, V. Microstructure Mechanisms Governing the Creep Life of Ultrafine-grained Cu-0.2wt.%Zr Alloy. *Acta Phys. Pol.* **2012**, *A 122*, 485–489.

9. Dvorak, J.; Kral, P.; Kvapilova, M.; Svoboda, M.; Sklenicka, V. Microstructure stability and creep behaviour of Cu-0.2wt.%Zr alloy processed by equal-channel angular pressing. *Mat. Sci. Forum* **2011**, *667–669*, 821–826. [CrossRef]
10. Sklenička, V.; Dvořák, J.; Král, P.; Svoboda, M.; Kvapilova, M.; Langdon, T. Factors influencing creep flow and ductility in ultrafine – grained metals. *Mater. Sci. Eng. A* **2012**, *558*, 403–411. [CrossRef]
11. Frost, H.J.; Ashby, M.F. *Deformation-Mechanism Maps*; Pergamon Press: Oxford, UK, 1982.
12. Neishi, K.; Horita, Z.; Langdon, T.G. Achieving superplasticity in ultrafine-grained copper: influence of Zn and Zr additions. *Mater. Sci. Eng. A* **2003**, *352*, 129–135. [CrossRef]
13. Li, Y.; Zeng, X.; Blum, W. Transition from strengthening to softening by grain boundaries in ultrafine-grained Cu. *Acta Mater.* **2004**, *52*, 5009–5018. [CrossRef]
14. Amouyal, Y.; Divinski, S.; Estrin, Y.; Rabkin, E. Short-circuit diffusion in an ultrafine-grained copper–zirconium alloy produced by equal channel angular pressing. *Acta Mater.* **2007**, *55*, 5968–5979. [CrossRef]
15. Wongsa-Ngam, J.; Wen, H.; Langdon, T.G. Microstructural evolution in a Cu–Zr alloy processed by a combination of ECAP and HPT. *Mater. Sci. Eng. A* **2013**, *579*, 126–135. [CrossRef]
16. Blum, W. High-Temperature Deformation and Creep of Crystalline Solids. In *Plastic Deformation and Fracture of Materials*; Mughrabi, H., Ed.; VCH Verlagsgesellschaft: Weinheim, Germany, 1993; pp. 359–405.
17. Reppich, B. Particle Strengthening. In *Plastic Deformation and Fracture of Materials*; Mughrabi, H., Ed.; VCH Verlagsgesellschaft: Weinheim, Germany, 1993; pp. 311–357.
18. Li, Y.J.; Mueller, J.; Höppel, H.; Göken, M.; Blum, W. Deformation kinetics of nanocrystalline nickel. *Acta Mater.* **2007**, *55*, 5708–5717. [CrossRef]
19. Mukherjee, A.; Bird, J.; Dorn, J. Experimental Correlations for High-Temperature Creep. *ASM Trans. Q.* **1969**, *62*, 155–179.
20. Čadek, J. *Creep in Metallic Materials*; Elsevier: Amsterdam, The Netherlands, 1988.
21. Kassner, M.; Pérez-Prado, M.T. Five-Power-Law Creep in Single Phase Metals and Alloys. *Prog. Mater. Sci.* **2000**, *45*, 1–102. [CrossRef]
22. Blum, W.; Eisenlohr, P. A simple dislocation model of the influence of high-angle boundaries on the deformation behavior of ultrafine-grained materials. In *15th International Conference on the Strength of Materials (ICSMA-15)*; IOP Publishing: Bristol, UK, 2010; Volume 240, pp. 1–4. [CrossRef]
23. Ghosh, A.K.; Raj, R. Grain size distribution effects in superplasticity. *Acta Metall.* **1981**, *29*, 607–616. [CrossRef]
24. Blum, W.; Dvořák, J.; Král, P.; Eisenlohr, P.; Sklenička, V. Effect of grain refinement by ECAP on creep of pure Cu. *Mater. Sci. Eng. A* **2014**, *590*, 423–432. [CrossRef]
25. Eisenlohr, P.; Blum, W. Maximal strain rate sensitivity of quasi-stationary deformation strength when subgrain size matches grain size. *J. Mater. Sci. Technol.* under review.
26. Blum, W.; Dvořák, J.; Král, P.; Sklenička, V. Dynamic grain coarsening in creep of pure Cu at 0.42 Tm after predeformation by ECAP. *Mater. Sci. Eng. A* **2018**, *731*, 520–529. [CrossRef]
27. Blum, W.; Zeng, X.H. A simple dislocation model of deformation resistance of ultrafine-grained materials explaining Hall–Petch strengthening and enhanced strain rate sensitivity. *Acta Mater.* **2009**, *57*, 1966–1974; Corrigendum to **2011**, *59*, 6205–6206. [CrossRef]